SCIENTIFIC REPORTS

OPEN

SUBJECT AREAS:
IMPLANTS
BIOMEDICAL MATERIALS

Received
1 April 2014

Accepted
1 August 2014

Published
22 August 2014

Correspondence and requests for materials should be addressed to X.L. (cisarli@zju.edu.cn)

* These authors contributed equally to this work.

The construction of hierarchical structure on Ti substrate with superior osteogenic activity and intrinsic antibacterial capability

Ying Huang[1,2]*, Guangyu Zha[1]*, Qiaojie Luo[1], Jianxiang Zhang[3], Feng Zhang[1], Xiaohui Li[3], Shifang Zhao[1], Weipu Zhu[4] & Xiaodong Li[1]

[1]Department of Oral and Maxillofacial Surgery, The Affiliated Stomatology Hospital, College of Medicine, Zhejiang University, Hangzhou 310006, P. R. China, [2]Department of Geriatric Dentistry, Peking University School and Hospital of Stomatology, Beijing 100081, P. R. China, [3]Department of Pharmaceutics, College of Pharmacy, Third Military Medical University, Chongqing 400038, P. R. China, [4]Department of Polymer Science and Engineering, Zhejiang University, Hangzhou 310027, P. R. China.

The deficient osseointegration and implant-associated infections are pivotal issues for the long-term clinical success of endosteal Ti implants, while development of functional surfaces that can simultaneously overcome these problems remains highly challenging. This study aimed to fabricate sophisticated Ti implant surface with both osteogenic inducing activity and inherent antibacterial ability simply via tailoring surface topographical features. Micro/submciro/nano-scale structure was constructed on Ti by three cumulative subtractive methods, including sequentially conducted sandblasting as well as primary and secondary acid etching treatment. Topographical features of this hierarchical structure can be well tuned by the time of the secondary acid treatment. Ti substrate with mere micro/submicro-scale structure (MS0-Ti) served as a control to examine the influence of hierarchical structures on surface properties and biological activities. Surface analysis indicated that all hierarchically structured surfaces possessed exactly the same surface chemistry as that of MS0-Ti, and all of them showed super-amphiphilicity, high surface free energy, and high protein adsorption capability. Biological evaluations revealed surprisingly antibacterial ability and excellent osteogenic activity for samples with optimized hierarchical structure (MS30-Ti) when compared with MS0-Ti. Consequently, for the first time, a hierarchically structured Ti surface with topography-induced inherent antibacterial capability and excellent osteogenic activity was constructed.

Titanium (Ti) and its alloys have been used extensively to fabricate implantable devices such as joint prostheses, facture fixation devices, and dental implants[1]. Although great success has been made, failures still occur mainly due to deficient osseointegration and implant-associated infections[2–4]. Therefore, there is particular interest to engineer surfaces that combine improved osseointegration capability and reduced infection risks. Unfortunately, the requirements for inhibiting bacteria adhesion and promoting osteogenic cell functions on implant surfaces cannot be simultaneously achieved by previously reported methods, mainly due to limitations of the applied strategies for surface modification[2]. For instance, whereas functionalization of the implant with antimicrobial agents is effective to inhibit bacterial adhesion, they may significantly compromise osteogenic cell functions[5]. On the other hand, incorporation of inorganic antibacterial agents can even induce severe cytotoxicity[6]. Currently, development of facile and reliable modification strategies that can endow surfaces with enhanced osteogenic activity and antibacterial ability remains highly challenging, despite its great value from the viewpoint of scientific significance and clinic applications.

Numerous earlier studies have shown that surface topographical features of a Ti substrate significantly affect its osteogenic inducing ability. The typical surface topography pattern on Ti implant is micro/submicro-scale structure that has been proved to be effective to promote pre-osteoblasts differentiation and extracellular matrix mineralization *in vitro* as well as new bone formation *in vivo*[7,8]. However, biological performances of the Ti implant with such surface topography pattern are not entirely satisfactory. Firstly, the enhanced differentiation behaviors of pre-osteoblasts on these surfaces are generally at the cost of reduced osteogenic cell adhesion and proliferation behaviors, whereas the latter is necessary to guarantee the quantity of newly formed bone tissues[9].

Secondly, their capacity of inducing osteogenic cell differentiation also needs to be further improved. Creating advanced surface topography patterns on Ti with further improved cellular responses for osteogenic cells is greatly desirable. Decorating a Ti implant surface with hierarchical structures via combining micro/submicro-scale structures with additional nanoscale structures may be one of the most attractive solutions. It is well accepted that nanoscale structures are potential stimuli for cell-surface interactions[10]. Also, it was reported that nanoscale structures on Ti surfaces could selectively increase the adhesion and proliferation behaviors of pre-oesteoblasts, but not fibroblasts[11]. To some extent, surface structures on Ti at nanoscale could also modulate the differentiation behaviors of pre-oesteoblasts[12]. Together with the benefits of micro/submicro-scale and nanoscale structures, hierarchical structures are believed to be more advantageous in biomedical applications by modulating cell behaviors at a multi-scale level[13–15].

Infection is a major problem in orthopedics leading to implant failure[16]. Once a bacterial bio-film has formed, it is difficult to treat and may eventually lead to the removal of the implant. Therefore, one approach to minimize implant-associated infections is to reduce the initial bacterial adhesion and colonization on the implant surfaces[17]. The traditional point of view considers that anti-adhesive polymers or antibacterial agents that are directly grafted on the implant surface are indispensable for inhibiting bacteria colonization on substrata[4,5,18]. Differently, some naturally occurring biological structures efficiently resist bacteria adhesion simply by their special surface topography. For instance, nano-patterned topographical feature on the Cicada wing surface could even kill the contacted bacteria based solely on its physical structures[19]. Although the mechanism by which surface topography modulates bacteria attachment remains largely unclear, this phenomenon revealed the possibility of minimizing or preventing bacteria colonization by tailoring surface topographical features. Up to date, anti-bacterial capacities for Ti surfaces merely via modulating surface topography have not been achieved. Moreover, no attempt has been made to exploit surface structures on Ti implants with dual functions of antibacterial ability and osteogenic inducing activity, although they are highly desirable in orthopedics.

To overcome the challenge of the situations mentioned above, a well arranged, novel hierarchical surface topography pattern model was exploited on Ti substrate in this study. Successive subtractive methods were used to create structures at various scales, i.e. microscale structure caused by sandblasting, submicroscale structure offered by a primary acid etching, and nanoscale structure produced by a secondary acid etching. Topographical features of this hierarchical structure can be well tuned by the time of the secondary acid etching. Interesting enough, a type of sophisticated, hierarchically structured Ti surfaces with topography-induced inherent antibacterial capability was found. On this basis, for the first time, a microstuctured Ti surface with topography-induced antibacterial ability and excellent osteogenic inducing activity was screened out via *in vitro* and *in vivo* biological tests.

Results

Surface topography of various Ti discs. Figure 1 showed the surface topography of Ti discs undergoing two or three successive subtractive treatments. The big pits with dozens of micrometers were offered by the trace of sandblasting, and the irregular crater-like holes with several micrometers or sub-micrometers were due to the first fierce acid etching with boiling H_2SO_4/HCl mixture, while the nanoscale structures resulted from the tender secondary acid etching with H_2SO_4/H_2O_2 mixture at room temperature. As can be seen in the MS0-Ti group (without secondary acid etching), big pits successively appeared on the sample surface, full of irregular and crater-like holes. The high resolution images indicated that ridges and valleys of the crater-like structures were essentially smooth (Fig. 1a, MS0-Ti). For the MS15-Ti ~ MS120-Ti groups (Ti substrata undergoing secondary acid etching from 15 to 120 min), big pits at micro-scale level could also be observed (the left panels of Fig. 1b–e). However, the depth of the crater-like holes gradually shoaled when the secondary acid-etching time increased (the middle panels of Fig. 1b–e). The crater-like structure almost disappeared when the treatment time was longer than 90 min. Meanwhile, nanostructure appeared on the ridges and valleys of the crater-like structure, and this structure became clear with the prolonged secondary acid etching (the right panels of Fig. 1b–e). Thus, for these hierarchical structures, the enhancement in nanostructure was accompanied with the weakening of micro- and submicro-structures.

Surface roughness. For surface modification of Ti implants, roughness has been introduced to enhance the geometric area for improved osteointegration[20]. The arithmetical mean deviations of the roughness profile (Ra) for various Ti samples were shown in Figure 2a. The Ra value of samples in the MS0-Ti group was 2.247 $\pm$ 0.137 μm, while that of other MS-Ti groups slowly decreased with the prolonged secondary acid etching treatment.

XRD patterns. XRD patterns of various Ti discs were illustrated in Figure 2b. Similar patterns with typical Ti peaks could be observed for smoothed Ti discs (SM-Ti) and nanostructured Ti (AE-Ti, SM-Ti further treated with H_2SO_4/H_2O_2 mixture at room temperature for 1 h). However, MS0-Ti showed typical Ti and TiH_2 (JCPDS#25-982) peaks after sandblasting and acid etching with H_2SO_4/HCl mixture, which was also reported previously[21]. Interestingly, surfaces of MS15-Ti ~ MS120-Ti groups exhibited almost the same XRD patterns as that of MS0-Ti. None of them displayed peaks corresponding to crystals of titanium oxide such as anatase or rutile phases.

XPS spectra. Figure 2c showed XPS spectra of Ti discs with various topological structures. For all surfaces, a strong doublet peak with broad shoulders appeared at about 458.7 and 464.3 eV. This peak should be attributed to Ti^{4+}, indicating that TiO_2 is the main constituent of the oxidized layer[22]. Deconvolution of the Ti^{2p} peak of MS0-Ti ~ MS120-Ti revealed that $Ti^{metallic}$ peaks (at 454.1 and 460.2 eV) gradually weakened with increase in the secondary acid-etching time. It has been reported that $Ti^{metallic}$ peaks are attributed to the underlying Ti substrate because of the thin oxide layer[23]. These results suggested all the MS-Ti samples were covered by an amorphous TiO_2 layer, and the thickness of this TiO_2 layer was increased with the secondary acid-etching treatment.

Contact angle and surface energy. The water contact angle and diiodomethane contact angle for a freshly prepared micro/submicro-scale structured surface (MS0-Ti) was about 6.0 $\pm$ 1.7° and 5.0 $\pm$ 1.5°, respectively, indicating that this surface was both hydrophilic and oleophilic (Table 1). Surprisingly, after incorporation of the nanoscale structure, water and diiodomethane droplet spread out fast on the micro/submicro/nano-scale structured surfaces (MS15-Ti ~ MS120-Ti groups), resulting in a contact angle of 0°. These results lead to the conclusion that construction of hierarchical structures on Ti could create surfaces that are highly hydrophilic and highly oleophilic (Table 1). Owens-Wendt method[24] was used to calculate surface free energy (SFE) according to the water and diiodomethane contact angles of the samples. For MS0-Ti, the SFE was 80.48 mJ/m^2, which was higher than that of SM-Ti and AE-Ti (Table S3&S4). As both the water and diiodomethane contact angle was 0° on the surface of MS15-Ti ~ MS120-Ti, their SFE values could not be calculated by the Owens-Wendt method (Table 2), and therefore these samples are of higher surface energy than MS0-Ti.

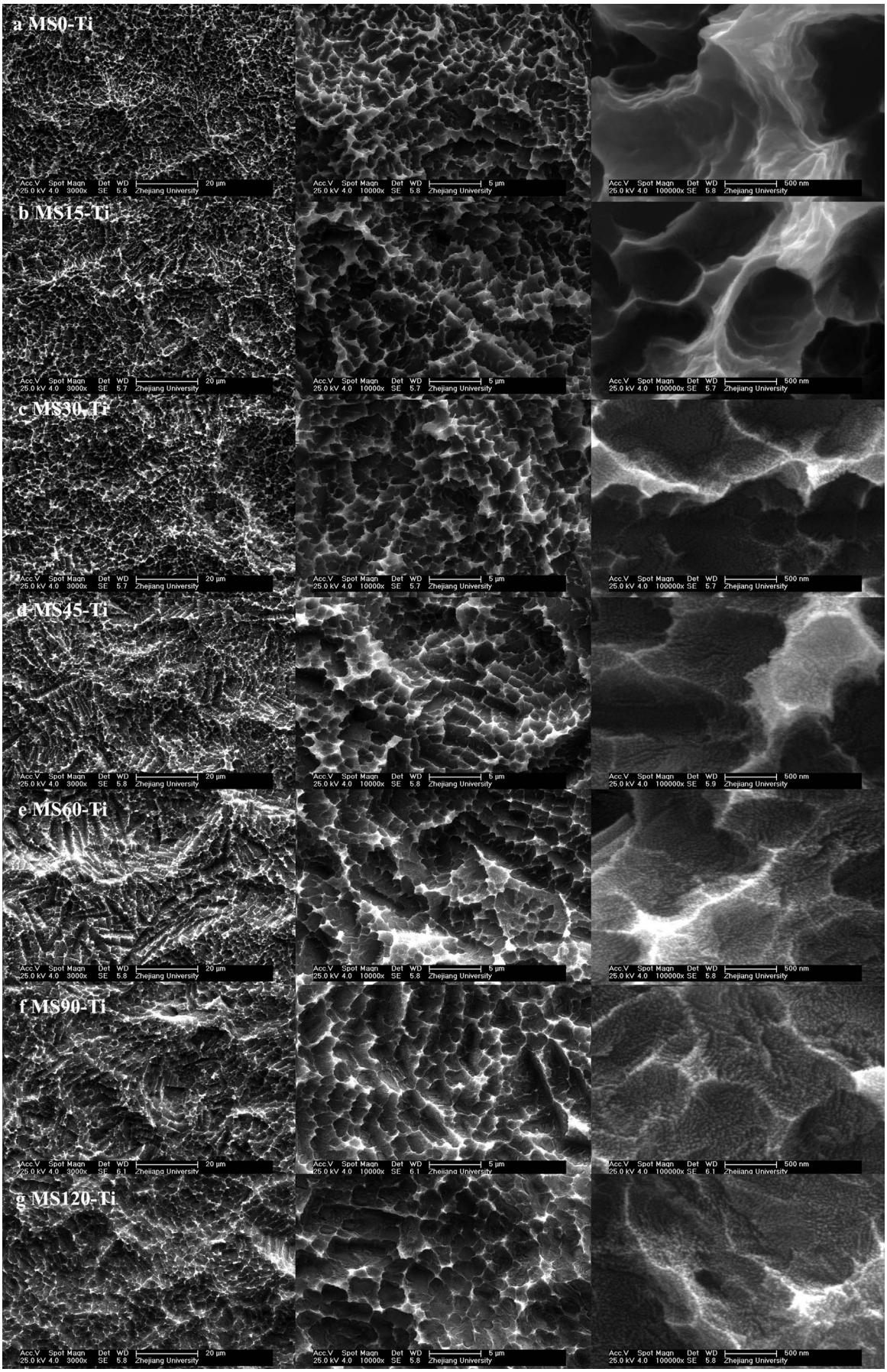

Figure 1 | SEM images of various Ti samples. (a) MS0-Ti; (b) MS15-Ti; (c) MS30-Ti; (d) MS60-Ti; (e) MS90-Ti; and (f) MS120-Ti.

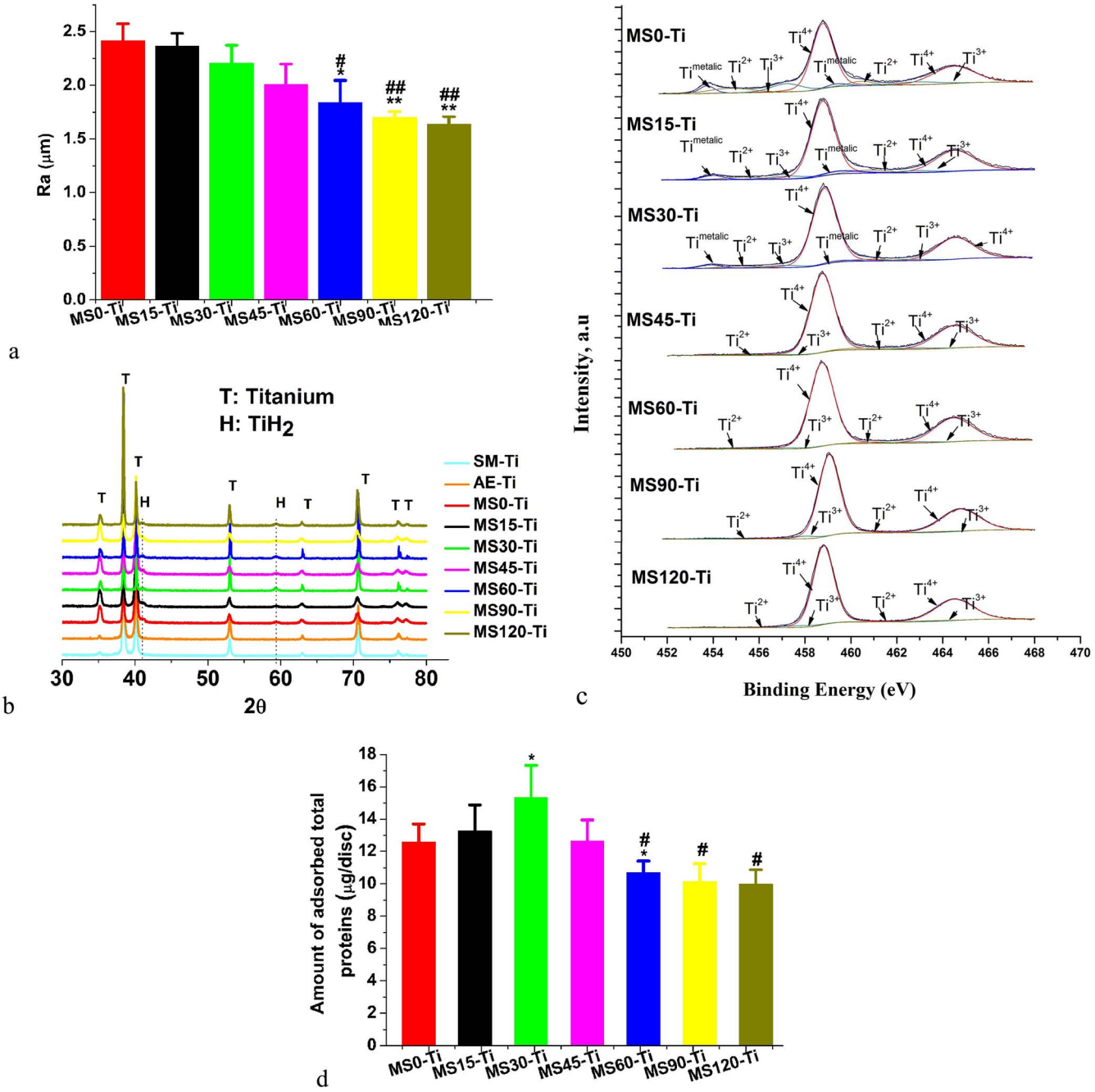

Figure 2 | (a) Surface roughness (Ra) of different groups. (b) XRD patterns of Ti samples. SM-Ti represents smoothed Ti samples and AE-Ti denotes smoothed and nano-patterned Ti samples. (c) Deconvolution of the Ti^{2p} peak in XPS profiles for MS-Ti groups. (d) Total protein adsorption behaviors for different groups. Data represent mean ± standard deviation (n = 3) with statistical difference (*, #, $p < 0.05$; **, ##, $p < 0.01$). The symbol * represents samples in the other groups versus the MS0-Ti group; symbol # represents samples in other groups versus that in MS30-Ti group.

Adsorption of total proteins. As illustrated in Figure 2d, the amount of total proteins adsorbed on MS0-Ti, MS15-Ti, and MS30-Ti was increased with the secondary acid-etching treatment time. However, further prolonged treatment unexpectedly gradually decreased the amount of adsorbed proteins on other groups from MS45-Ti to MS120-Ti, and the amount on MS60-Ti was even lower than that on MS0-Ti ($p < 0.05$). The amount of adsorbed proteins and their conformational states are largely controlled by the implant surface

Table 1 | Contact angle of different Ti substrates

Groups		MS0-Ti	MS15-Ti	MS30-Ti	MS45-Ti	MS60-Ti	MS90-Ti	MS120-Ti
Contact angle (n = 5)	Water	6° (1.7°)	0°	0°	0°	0°	0°	0°
	Diiodomethane	5° (1.5°)	0°	0°	0°	0°	0°	0°

Table 2 | Surface free energy calculated according to Owens-Wendt method[24]

Groups	MS0-Ti	MS15-Ti	MS30-Ti	MS45-Ti	MS60-Ti	MS90-Ti	MS120-Ti
γ^p (mJ/m^2)	50.78	_a	_a	_a	_a	_a	_a
γ^d (mJ/m^2)	30.61	_a	_a	_a	_a	_a	_a
γ (mJ/m^2)	81.39	_a	_a	_a	_a	_a	_a

[a]Can not be calculated due to spreading (contact angle 0°) of some liquids. Spreading indicates high energy surfaces.

properties. Since factors such as surface chemistry, surface wettability, and surface energy that may affect protein adsorption behaviors[25] are similar in the MS0-Ti and MS15 ~ 120-Ti groups, specific surface area would be a decisive factor for protein adsorption behaviors of the MS-Ti groups.

It could be seen from Figure 2d that protein adsorption ability of MS30-Ti was the highest among all the MS-Ti samples. Further increase or decrease in the treatment time of the secondary acid-etching impaired the adsorption capability. This phenomenon revealed that the increased surface area caused by the enhanced nanoscale structures might be partly balanced out by the weakening of micro and submicro-scale structures with the prolonged secondary acid-etching (Fig. 1b–e). MS30-Ti possessed the largest specific surface area. According to SEM observation, roughness measurement, and protein adsorption assay, the groups of MS0-Ti, MS30-Ti, and MS60-Ti, which represented the typical surface topography and property evolution in MS-Ti groups as the secondary acid-etching treatment time prolonged, were selected for further biological evaluations.

Antibacterial assay. The influence of the surface topographical features on the initial adhesion of *E. coli* and *S. aureus* cells on tested Ti substrates was examined by cell-counting assay and SEM observation (Fig. 3). Counting scores of the adherent bacterial cells were significantly different among tested groups (Fig. 3a, b, c). At 0.5 h, the initial stage of bacteria-substrate contact, less *E. coli* and *S. aureus* adhered on MS30-Ti and MS60-Ti surfaces than that on MS0-Ti. At 6 h, *E. coli* proliferated fast on MS0-Ti and its number was nine-fold higher than that at 0.5 h. The proliferation of *E. coli* on MS30-Ti and MS60-Ti surfaces at 6 h was dramatically suppressed and its number was similar to that at 0.5 h. At 6 h, *S. aureus* also proliferated fast on the groups including MS0-Ti, MS30-Ti, and MS60-Ti, and its cell number was 18.6, 8.5, and 4.3 times more than that at 0.5 h, respectively (Fig. 3b, c). These results indicated that MS30-Ti and MS60-Ti exhibited the ability of inhibiting initial adhesion and colonization of both *E. coli* and *S. aureus* cells, and *E. coli* was more sensitive to the topography-induced antibacterial effects contributed by the constructed hierarchical structure. Furthermore, Figure 3a showed that the binary fission (white arrow) of *E. coli* and *S. aureus* could be easily observed on the surface of MS0-Ti group after 6 h of culture, while almost no binary fission state of *E. coli* and *S. aureus* could be found on the surfaces of MS30-Ti and MS60-Ti. Bacterial cells on MS0-Ti displayed smooth and intact grape-shape (*S. aureas*) and rod shape (*E. coli*), while obviously damaged shapes, such as irregular cell rim and sucking cavity-like deformation were observed on both MS30-Ti and MS60-Ti, which was shown by yellow dotted lines and arrows in Fig. 3d.

Cell morphology. Figure 4 showed the morphology change and cytoskeleton organization of pre-osteoblasts on various Ti surfaces after 1, 4, and 24 h of culture. Most cells on the samples of MS0-Ti were disc-like while almost cells on the samples of MS30-Ti and MS60-Ti were star-like after 1 h of culture. Furthermore, abundant filopodia attachment, which acts as the environmental sensor and traction elements[10], was found on samples of MS30-Ti and MS60-Ti. Cells on all the samples spread with the increased culture time in all groups. After 4 h of culture, cell processes of those disc-like cells on the samples of MS0-Ti began to form while most cells on the samples of MS30-Ti and MS60-Ti have already displayed polygon-like morphology. After 24 h of cell culture, cell processes of pre-osteoblasts on the samples of MS30-Ti and MS60-Ti was more spreading than those needle-like processes on the samples of MS0-Ti. This phenomenon implied that cells on hierarchically structured surfaces of MS30-Ti and MS60-Ti spread more efficiently than that on the micro/submicron surface of MS0-Ti at all the time points. Especially for the hierarchical structure of MS60-Ti, even larger cell spread area than those of other two groups could be found at 24 h. As well documented, cells respond to particular biochemical and physical properties of the microenvironment by initiating a cascade of events, including the activation of phosphorylation and G protein mediated pathways, which result in local alterations in cytoskeletal dynamics and the generation of mechanical force[26]. In this study, it seemed that there still was unambiguous stress fibers for cells cultured in the MS0-Ti group for 24 h, while there was gradually distinct stress fibers for cells cultured on MS30-Ti and MS60-Ti for 24 h. These results revealed that the cell adhesion behaviors on the micro/submicron surface were improved with the introduction of additional nanoscale structure, resulting in cell morphology change, formation of filopodia, and accelerated cytoskeleton reorganization.

Cell proliferation. Cell proliferation assay of pre-osteoblasts showed that there was no significant difference in the number of cells attached to the sample surface among the three groups at 1 h (Fig. 5a). Among various MS-Ti groups, the cell proliferation capacity enhanced as the secondary acid-etching time increased, characterized by the highest cell number in the MS60-Ti group and the lowest in the MS0-Ti group on both day 3 and day 7 ($p < 0.05$).

Osteogenic differentiation phenotype expression. Besides the initial cellular attachment and proliferation, the subsequent ALP activity and calcium deposition are critical factors for enhancing osseointegration. It was reported that ALP is specifically synthesized by osteogenic cells at the early stage of differentiation[27,28]. At all the tested time points, the MS30-Ti group exhibited improved ALP activity in comparison to the MS0-Ti group ($p < 0.05$), while ALP activity of cells in the MS60-Ti group was inferior to that of the MS0-Ti group (Fig. 5b).

OC, a marker for late differentiation of pre-osteoblast cells, was measured after the cells were cultured for two weeks on different substrata[29]. The amount of OC produced on MS30-Ti and MS60-Ti was 1.6 and 2.6 times higher than that on MS60-Ti at week 2, respectively (Fig. 5c).

The effect of surface topography on the expression levels of bone-specific genes *Akp-2* and *OC* was also examined. MS30-Ti showed greatly up-regulated mRNA expression levels of both *Akp-2* and *OC* when compared with MS0-Ti (Fig. 5d–e) at all time points ($p < 0.05$). However, for the MS60-Ti group, the osteogenic gene expression was lower than that of the MS0-Ti group ($p < 0.05$).

Biomechanical test. RTQ test was performed to investigate the biomechanical stability of Ti implants. The bone-Ti interfacial

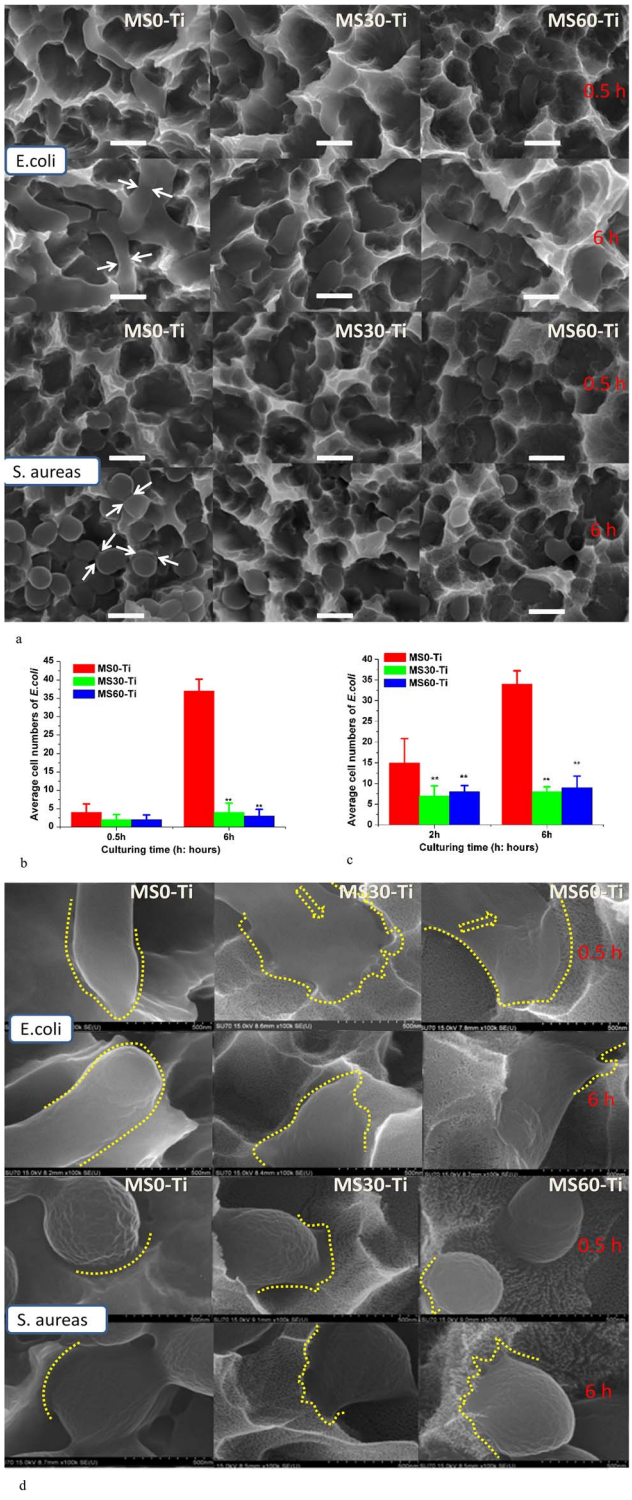

Figure 3 | SEM images of E. coli and S. aureus on different Ti surfaces after 0.5 and 6 h of culture and the results of cell-counting assay. (a) SEM images of E. coli and S. aureus on different Ti surfaces under low magnification, white arrow indicates the binary fission of bacteria, scale bar = 1 μm. (b) Cell-counting score of E. coli. (c) Cell-counting score of S. aureus. Data represent mean ± standard deviation (n = 10) with statistical difference (*, $p < 0.05$; **, $p < 0.01$). The symbol * represents samples in other groups versus that in the MS0-Ti group. (d) SEM images of E. coli and S. aureus on different Ti surfaces under high magnification, which aimed to show the intact, damaged morphology of bacteria. Yellow dotted lines showed the intact sphere rim of S. aureus and rod shape of E. coli on MS0-Ti, but demonstrated irregular deformed morphology of E. coli and S. aureus in MS30-Ti and MS60-Ti groups. The dotted arrows showed abnormal pits in the bacterial cells.

binding strength was determined through a biomechanical test. At each tested time point, the MS30-Ti-implant group showed an increased bone-to-implant binding strength compared with the MS0-Ti-implant group (Fig. 6), and there is statistical difference between these two groups at week 2 ($p < 0.05$). However, for the MS60-Ti-implant, the binding strength at each tested time point was lower than that of the MS30-Ti-implant ($p < 0.05$), and even lower than that of the MS0-Ti-implant group ($p < 0.05$).

Discussion

It remains challenging to engineer Ti implant surfaces that may improve osseointegration and simultaneously reduce infection risks, in view of the fact that the introduction of antibacterial coatings or substances frequently causes the unfavorable effects on osteogenic cell functions. In this study, for the first time it was amazing but authentic to find that the resultant micron/submicron/nano-structures fabricated on Ti displayed excellent osteogenic-inducing activity and remarkable intrinsic anti-bacterial adhesion ability, simply by tailoring topographical features. The construction of hierarchical structure alternated the surface physicochemical properties of Ti, which were responsible for the prominent biological effects.

In this context, surface topographical features of the multi-scale structure could be modulated by adjusting the duration of exposure to the H_2SO_4/H_2O_2 mixture. As a result, a series of hierarchical surface topographical patterns were created (Fig. 1). XPS detection revealed that Ti^{4+} contributed to the main component of the out layer of all the MS-Ti surfaces (Fig. 2c). It is well known that three types of titanium dioxides can be found in the nature, including anatase, rutile, and amorphous titanium dioxide[30]. Since all the MS-Ti samples did not showed any anatase or rutile peaks in the XRD spectra (Fig. 2d), we can conclude that they were covered by a super-thin layer of amorphous titanium dioxide. These results suggested that surface chemistry of all MS-Ti surfaces kept high conformity although a secondary acid-etching treatment was applied to create superimposed nano-scale structures. The consistency in surface chemistry allowed the examination of pure topographical effects on osteogenic inducing activity and antibacterial ability.

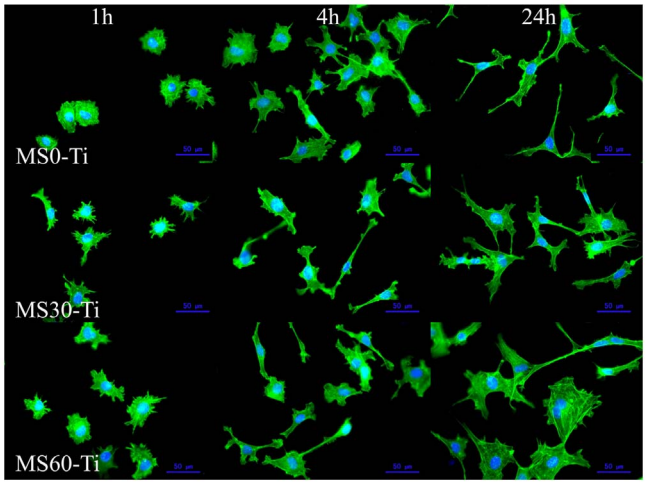

Figure 4 | Cell morphology on various structures after 1, 4, or 24 h of culture. The actin and nuclear were stained with FITC-phalloidin and Hoechst 33342, respectively. Scale bar = 50 μm.

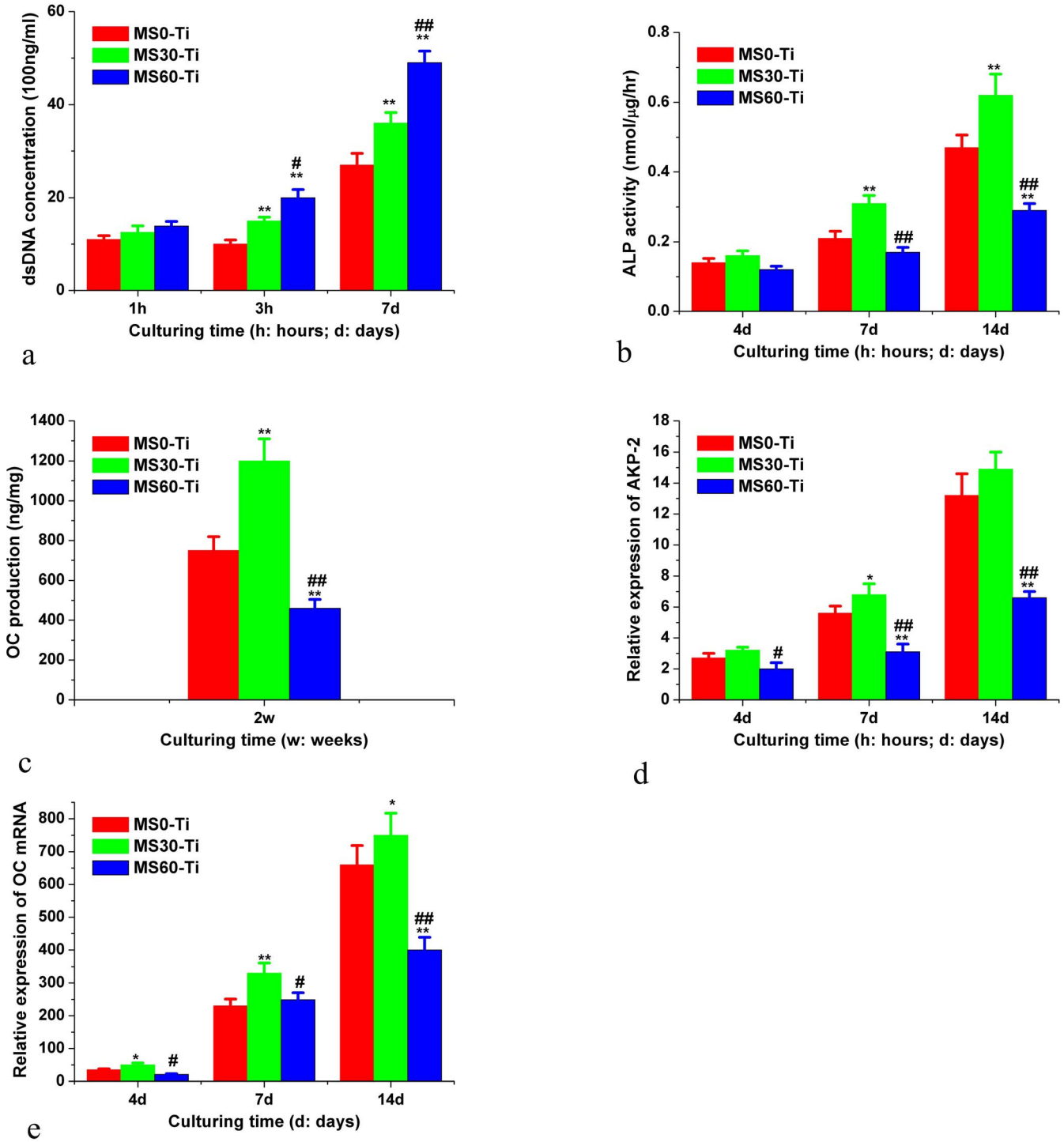

Figure 5 | **Osteogenic activities of various surfaces.** (a) Cell attachment and proliferation; (b) ALP activity; (c) OC production; (d) AKP-2 mRNA expression; and (e) OC mRNA expression. Data represent mean ± standard deviation (n = 3) with statistical difference (*, $^{\#}$, $p < 0.05$; **, $^{\#\#}$, $p < 0.01$). The symbol * represents samples in the other groups versus that in the MS0-Ti group; symbol $^{\#}$ represents samples in other groups versus that in MS30-Ti group.

In terms of implant-associated infections, once occurring, bacteria tend to aggregate in a hydrated polymeric matrix to form a bio-film on the implant surface that is hardly to be destroyed[31]. Thus, the first 6 hours is the "decisive period"[32] to interfere with the microbial colonization process on the Ti implants. Previous studies revealed that the reduction of bacteria adhesion on the biomaterial surface led to a markedly reduction in bio-film formation[33,34]. In this manuscript, results of SEM observation and cell counting (Fig. 3) revealed that at the early stage of bacteria-Ti interactions, the micro/submicro/nano-scale structures generated in this study markedly reduced bacteria adhesion and alternated cell morphology of both gram-negative and gram-positive bacteria when compared to that on the micro/submicron-scale structures. The decreased number of adhered bacteria on the hierarchical structure might be attributed to the presence of the additional nanoscale structure (less than 100 nm) that inhibited the preliminary steps of bacteria adhesion

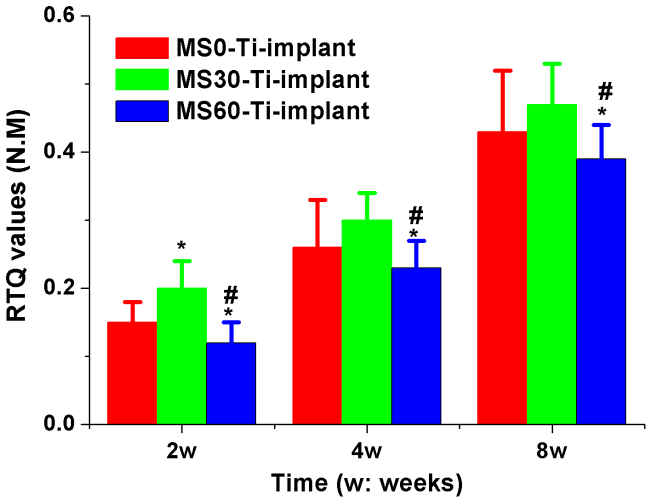

Figure 6 | Removal torque tests at 2, 4, and 8 weeks after implantation. The MS0-Ti-implant, MS30-Ti-implant, and MS60-Ti-implant are Ti implants duplicating the topological structure features of MS0-Ti, MS30-Ti, and MS60-Ti, respectively. Data represent mean ± standard deviation (n = 6) with statistical difference (*, #, $p < 0.05$). The symbol * represents samples in the other groups versus that in the MS0-Ti-implant group; symbol # represents samples in other groups versus that in MS30-Ti-implant group.

via reducing the available substrata-bacteria contact area[35]. Moreover, for bacteria adhered on the substrata with hierarchical structures, obvious membrane deformation could be observed in contrast to that on the micro/submicro-scale structures. This might be associated with the high surface free energy and super-amphiphilicity of the surface in MS30-Ti and MS60-Ti groups. The membrane deformation of bacteria may be induced in order to balance the high energy gained due to adsorption on the hierarchical surface[19], leading to suppressed or damaged cell functions (e.g., reduced binary fission). Obviously, in-depth studies are needed to address the exact antibacterial mechanism. Herein, the hierarchically micro/submicro/nano-structured super-amphiphilic Ti surface with high surface free energy exhibited a topography-induced antibacterial ability, which demonstrated a novel bacteria-Ti implant interaction pattern.

The inherent antibacterial capacity of hierarchical structures avoids the drawbacks of extrinsic antibacterial reagents that may affect rapid and robust osteointegration, which include the use of organic coatings such as chitosan or silk on Ti to attain temporary antibacterial effects[36,37], or using inorganic nanoparticles[6], while the later frequently leads to potential toxicity to eukaryotic cells of peri-implant tissues. Moreover, the hierarchical surface topographical feature and its super-amphiphilicity and high surface free energy may be favorable to its osteogenesis inducing ability.

The introduced nano-scale structures produced sophisticated surface properties, such as the increased surface area that benefited protein adsorption and the super-amphiphilicity and high surface energy that enhanced the cell-to-substrata affinity[38], which may play important roles in the achieved biological performance. Moreover, cells are able to respond to nano-scale structures, since *in vivo* they live inside an extracellular matrix (ECM) containing nano-scale collagen fibrils and their own surface is structured at the nano-scale level (receptors and filopodia)[10,39]. Immunofluorescence assay (Fig. 4) exhibited consistent results that improved pre-osteoblasts adhesion behaviors could be observed on the samples with additional nano-scale structures, showing more filopodia attachment and better spreading of pre-osteoblasts. Cellular adhesion provides environmental cues that influence cellular decisions for proliferation and differentiation and this is a critical initial step in the formation of cellular-substrata interactions[40,41]. Accordingly, dsDNA quantification analysis (Fig. 5a) demonstrated the enhanced proliferation behaviors of pre-osteoblasts on the surfaces of MS30-Ti and MS60-Ti, when compared with that of MS0-Ti. The phenomenon that the attachment and proliferation behaviors of pre-osteoblasts on MS60-Ti were enhanced while samples in this group adsorbed less total proteins when compared with MS30-Ti group, was interesting. The possible reason should be the clearly increased nano-scale structure in samples of MS60-Ti group. This phenomenon implied that together with the adsorbed proteins on hierarchical surfaces, nano-scale structure also participated in modulating adhesion behaviors of osteoblasts. Cell differentiation assay of both osteogenic protein and gene (Fig. 5b–e) confirmed the success of improving osteogenic cell differentiation via the introduction of superimposed nano-scale structures on micro/submicron scale structures (MS30-Ti group). Nevertheless, one can observe that if the introduced nano-scale structures excessively consumed the micro/submicron scale structures, the differentiation stimulating ability of the resulting hierarchical structure would be impaired (MS60-Ti group). The above-mentioned phenomena revealed the effectiveness of regulating surface topographical features to control cellular behaviors on the Ti substrata.

In vivo biomechanical stability of the MS0-Ti-implant, MS30-Ti-implant, and MS60-Ti-implant exhibited a similar trend as that of cell differentiation inducing ability. Biomechanical stability of rough-surfaced implants come from both the mechanical interlocking and the bone-to-implant biological fixation[42]. Three factors may account for the highest biomechanical stability of the MS30-Ti-implant group: the greatest specific surface area that increased the mechanical interlocking; the hierarchical topography features that provided multi-level cues for peri-implant tissue regeneration; and the surface characteristics of super-hydrophilicity and high surface energy that also partly contributed to the enhanced biological fixation[43]. Although the MS60-Ti-implant was also hierarchically structured, and displayed super-hydrophilicity and high surface energy, they displayed inferior biomechanical stability over the MS0-Ti-implant. This phenomenon could be attributed to the insufficient cell differentiation behaviors on the surface of MS60-Ti-implant.

In summary, obvious antibacterial ability and excellent osteogenic activity were simultaneously achieved via a carefully built hierarchical structure on Ti. In a previous study, super-hydrophobic hierarchical surfaces were found able to increase the bacteria contamination resistance on Ti for the reason that hydrophobic hierarchical surfaces possessed anti-fouling property due to the "lotus effects"[44]. Nevertheless, although such surfaces displayed reasonable antibacterial adhesion ability, they may not serve as the most appropriate candidate for implantable endosteal applications due to the fact that the hydrophobic surface with low surface energy displays irreversible protein adsorption behaviors and relative inferior peri-implant new bone formation ability[45]. Instead, the antibacterial hierarchical structure engineered in this study possessed super-amphiphilicity, strong protein adsorption capability, and high surface energy, promising the excellent osteogenic inducing activity of Ti substrata. Ti implants with such hierarchical surface are capable of simultaneous reducing infection risks and further improving osseointegration when compared with the clinically available implant systems, which may contribute to an improved long term clinical success of endosteal Ti implants.

Conclusion

In conclusion, a well-designed, hierarchically structured Ti surface with antibacterial ability and excellent osteo-conductivity was fabricated on Ti via a facile and reliable surface modification strategy, which was based on sequential subtractive treatments including sandblasting, a primary and a secondary acid etching treatments. A new bacteria-Ti substrate interaction pattern was found. This

study enhanced our understanding on the relationship between the Ti surface topographical feature and its biological properties, and accordingly may guide the exploitation of next generation dental implants using multiply subtractive treatments. This kind of hierarchical surface can also get wide application in the field of joint prostheses, facture fixation devices, and other permanent endosteal implants. Future studies will be conducted to investigate how the hierarchical structure features interact with bacteria in antibacterial behaviors and how they guide cellular/tissue responses in the process of osseointegration.

1. Liu, X., Chu, P. K. & Ding, C. Surface modification of titanium, titanium alloys, and related materials for biomedical applications. *Mater Sci Eng R* **47**, 49–121 (2004).
2. Neoh, K. G., Hu, X., Zheng, D. & Kang, E. T. Balancing osteoblast functions and bacterial adhesion on functionalized titanium surfaces. *Biomater* **33**, 2813–2822 (2012).
3. Zhao, L., Chu, P. K., Zhang, Y. & Wu, Z. Antibacterial coatings on titanium implants. *J Biomed Mater Res B* **91**, 470–480 (2009).
4. Huo, K. *et al*. Osteogenic activity and antibacterial effects on titanium surfaces modified with Zn-incorporated nanotube arrays. *Biomater* **34**, 3467–3478 (2013).
5. Zhang, F., Zhang, Z., Zhu, X., Kang, E.-T. & Neoh, K.-G. Silk-functionalized titanium surfaces for enhancing osteoblast functions and reducing bacterial adhesion. *Biomater* **29**, 4751–4759 (2008).
6. Zhao, L. *et al*. Antibacterial nano-structured titania coating incorporated with silver nanoparticles. *Biomater* **32**, 5706–5716 (2011).
7. Boyan, B. D. *et al*. Osteoblasts generate an osteogenic microenvironment when grown on surfaces with rough microtopographies. *Eur Cells Mater* **6**, 22–27 (2003).
8. Wilkinson, A. *et al*. Biomimetic microtopography to enhance osteogenesis in vitro. *Acta Biomater* **7**, 2919–2925 (2011).
9. Ogawa, T., Sukotjo, C. & Nishimura, I. Modulated bone matrix-related gene expression is associated with differences in interfacial strength of different implant surface roughness. *J Prosthodont* **11**, 241–247 (2002).
10. Biggs, M. J., Richards, R. G. & Dalby, M. J. Nanotopographical modification: a regulator of cellular function through focal adhesions. *Nanomedicine* **6**, 619–633 (2010).
11. Variola, F. *et al*. Tailoring the surface properties of Ti6Al4V by controlled chemical oxidation. *Biomater* **29**, 1285–1298 (2008).
12. Tambasco de Oliveira, P. & Nanci, A. Nanotexturing of titanium-based surfaces upregulates expression of bone sialoprotein and osteopontin by cultured osteogenic cells. *Biomater* **25**, 403–413 (2004).
13. Gittens, R. A. *et al*. The effects of combined micron-/submicron-scale surface roughness and nanoscale features on cell proliferation and differentiation. *Biomater* **32**, 3395–3403 (2011).
14. Zhao, L., Liu, L., Wu, Z., Zhang, Y. & Chu, P. K. Effects of micropitted/nanotubular titania topographies on bone mesenchymal stem cell osteogenic differentiation. *Biomater* **33**, 2629–2641 (2012).
15. Kubo, K. *et al*. Cellular behavior on TiO2 nanonodular structures in a micro-to-nanoscale hierarchy model. *Biomater* **30**, 5319–5329 (2009).
16. Heitz-Mayfield, L. J. Peri-implant diseases: diagnosis and risk indicators. *J Clin Periodontol* **35**, 292–304 (2008).
17. Zaborowska, M. *et al*. Bacteria-material surface interactions: methodological development for the assessment of implant surface induced antibacterial effects. *J Biomed Mater Res B* (2014).
18. Chua, P.-H., Neoh, K.-G., Kang, E.-T. & Wang, W. Surface functionalization of titanium with hyaluronic acid/chitosan polyelectrolyte multilayers and RGD for promoting osteoblast functions and inhibiting bacterial adhesion. *Biomater* **29**, 1412–1421 (2008).
19. Pogodin, S. *et al*. Biophysical model of bacterial cell interactions with nanopatterned cicada wing surfaces. *Biophys J* **104**, 835–840 (2013).
20. Rupp, F. *et al*. Enhancing surface free energy and hydrophilicity through chemical modification of microstructured titanium implant surfaces. *J Biomed Mater Res A* **76**, 323–334 (2006).
21. Perrin, D., Szmukler-Moncler, S., Echikou, C., Pointaire, P. & Bernard, J. P. Bone response to alteration of surface topography and surface composition of sandblasted and acid etched (SLA) implants. *Clin Oral Implan Res* **13**, 465–469 (2002).
22. Sittig, C., Textor, M., Spencer, N. D., Wieland, M. & Vallotton, P. H. Surface characterization of implant materials c.p. Ti, Ti-6Al-7Nb and Ti-6Al-4V with different pretreatments. *J Mater Sci Mater Med* **10**, 35–46 (1999).
23. Yi, J.-H. *et al*. Characterization of a bioactive nanotextured surface created by controlled chemical oxidation of titanium. *Surf Sci* **600**, 4613–4621 (2006).
24. Zhong, Z. *et al*. Surface energy for electroluminescent polymers and indium-tin-oxide. *Appl Surf Sci* **207**, 183–189 (2003).
25. Sela, M. N., Badihi, L., Rosen, G., Steinberg, D. & Kohavi, D. Adsorption of human plasma proteins to modified titanium surfaces. *Clin Ooral Implan Res* **18**, 630–638 (2007).
26. Geiger, B., Spatz, J. P. & Bershadsky, A. D. Environmental sensing through focal adhesions. *Nature reviews. Mol Cell Bio* **10**, 21–33 (2009).
27. Kartsogiannis, V. & Ng, K. W. Cell lines and primary cell cultures in the study of bone cell biology. *Mol Cell Endocrinol* **228**, 79–102 (2004).
28. Wang, Y. *et al*. Osteoblastic cell response on fluoridated hydroxyapatite coatings. *Acta Biomatera* **3**, 191–197 (2007).
29. Stein, G. S. & Lian, J. B. Molecular mechanisms mediating proliferation/differentiation interrelationships during progressive development of the osteoblast phenotype. *Endocr Rev* **14**, 424–442 (1993).
30. Nishiguchi, S. *et al*. Titanium metals form direct bonding to bone after alkali and heat treatments. *Biomater* **22**, 2525–2533 (2001).
31. Costerton, J. W., Stewart, P. S. & Greenberg, E. P. Bacterial biofilms: a common cause of persistent infections. *Science* **284**, 1318–1322 (1999).
32. Colon, G., Ward, B. C. & Webster, T. J. Increased osteoblast and decreased Staphylococcus epidermidis functions on nanophase ZnO and TiO2. *J Biomed Mater Res A* **78**, 595–604 (2006).
33. Xu, L. C. & Siedlecki, C. A. Submicron-textured biomaterial surface reduces staphylococcal bacterial adhesion and biofilm formation. *Acta Biomater* **8**, 72–81 (2012).
34. Ludecke, C. *et al*. Reproducible biofilm cultivation of chemostat-grown Escherichia coli and investigation of bacterial adhesion on biomaterials using a non-constant-depth film fermenter. *PloS one* **9**, e84837 (2014).
35. Yao, C., Webster, T. J. & Hedrick, M. Decreased bacteria density on nanostructured polyurethane. *J Biomed Mater Res A* (2013).
36. Zhang, F., Zhang, Z., Zhu, X., Kang, E. T. & Neoh, K. G. Silk-functionalized titanium surfaces for enhancing osteoblast functions and reducing bacterial adhesion. *Biomater* **29**, 4751–4759 (2008).
37. Shi, Z., Neoh, K. G., Kang, E. T., Poh, C. & Wang, W. Bacterial adhesion and osteoblast function on titanium with surface-grafted chitosan and immobilized RGD peptide. *J Biomed Mater Res A* **86**, 865–872 (2008).
38. Rupp, F. *et al*. Enhancing surface free energy and hydrophilicity through chemical modification of microstructured titanium implant surfaces. *J Biomed Mater Res Part A* **76A**, 323–334 (2006).
39. Decuzzi, P. & Ferrari, M. Modulating cellular adhesion through nanotopography. *Biomater* **31**, 173–179 (2010).
40. Bruinink, A. *et al*. Addition of nanoscaled bioinspired surface features: A revolution for bone-related implants and scaffolds? *J Biomed Mater Res A* (2013).
41. Powell, H. M., Kniss, D. A. & Lannutti, J. J. Nanotopographic control of cytoskeletal organization. *Langmuir* **22**, 5087–5094 (2006).
42. Le Guehennec, L., Soueidan, A., Layrolle, P. & Amouriq, Y. Surface treatments of titanium dental implants for rapid osseointegration. *Dental Maters* **23**, 844–854 (2007).
43. Zhao, G. *et al*. High surface energy enhances cell response to titanium substrate microstructure. *J Biomed Mater Res A* **74**, 49–58 (2005).
44. Fadeeva, E. *et al*. Bacterial Retention on Superhydrophobic Titanium Surfaces Fabricated by Femtosecond Laser Ablation. *Langmuir* (2011).
45. Buser, D. *et al*. Enhanced bone apposition to a chemically modified SLA titanium surface. *J Dent Res* **83**, 529–533 (2004).

Acknowledgments

This study was financially supported by the National Natural Science Foundation of China (51173163), the National Science-technology Support Plan project of China (2012BAI07B01) and the fundamental Research Funds for the Central Universities (2012QNA7043).

Author contributions

All authors contributed to the manuscript. X.D.L. designed study, supervised the study, analyzed data and co-wrote the manuscript. Y.H. performed most of the experiments and generated data and figures and co-wrote the manuscript. G.Y.Z. performed experiments and generated data and figures and co-wrote the manuscript. Q.J.L. and F.Z. performed experiments and generated and analyzed data. J.X.Z. and W.P.Z. generated methods and analyzed data. X.H.L. and S.F.Z. supervised the animal experiments. All authors reviewed the manuscript.

Additional information

Ethics statement Animal experiment was approved by the Zhejiang University Administration on Laboratory Animal Care. Animals were treated in accordance with Institutional Animal Care and Use Committee (IACUC) guidelines of Zhejiang University.

Supplementary information accompanies this paper at http://www.nature.com/scientificreports

Competing financial interests: The authors declare no competing financial interests.

How to cite this article: Huang, Y. *et al*. The construction of hierarchical structure on Ti substrate with superior osteogenic activity and intrinsic antibacterial capability. *Sci. Rep.* **4**, 6172; DOI:10.1038/srep06172 (2014).